Journal of Applied Physics

Spin pumping at interfaces with ferro- and paramagnetic $Fe_{60}Al_{40}$ films acting as spin source and spin sink

Cite as: J. Appl. Phys. **132**, 213906 (2022); https://doi.org/10.1063/5.0125699
Submitted: 13 September 2022 • Accepted: 29 October 2022 • Published Online: 02 December 2022

T. Strusch, K. Lenz, R. Meckenstock, et al.

Journal of Applied Physics ARTICLE scitation.org/journal/jap

Spin pumping at interfaces with ferro- and paramagnetic $Fe_{60}Al_{40}$ films acting as spin source and spin sink

Cite as: J. Appl. Phys. **132**, 213906 (2022); doi: 10.1063/5.0125699
Submitted: 13 September 2022 · Accepted: 29 October 2022 ·
Published Online: 2 December 2022

T. Strusch,[1] K. Lenz,[2] R. Meckenstock,[1] R. Bali,[2] J. Ehrler,[2] J. Lindner,[2] J. Fassbender,[2,3] M. Farle,[1] K. Potzger,[2] and A. Semisalova[1,a)]

AFFILIATIONS

[1]Faculty of Physics and Center for Nanointegration Duisburg-Essen (CENIDE), University of Duisburg-Essen 47057 Duisburg, Germany
[2]Helmholtz-Zentrum Dresden-Rossendorf, Institute of Ion Beam Physics and Materials Research, 01328 Dresden, Germany
[3]Institute of Solid State and Materials Physics, Technische Universität Dresden, 01069 Dresden, Germany

[a)]**Author to whom correspondence should be addressed:** anna.semisalova@uni-due.de

ABSTRACT

We present a study of spin pumping efficiency and determine the spin mixing conductance and spin diffusion length in thin bilayer films based on 3d transition metal alloy $Fe_{60}Al_{40}$. Due to its magnetostructural phase transition, $Fe_{60}Al_{40}$ can be utilized as a ferromagnetic (FM) or paramagnetic (PM) material at the same temperature depending on its structural order; thus a thin $Fe_{60}Al_{40}$ film can act as a spin source or a spin sink when interfaced with a paramagnet or a ferromagnet, respectively. Ferromagnetic resonance measurements were performed in a frequency range of 5–35 GHz on bilayer films composed of FM–$Fe_{60}Al_{40}$/Pd and PM–$Fe_{60}Al_{40}$/$Ni_{80}Fe_{20}$ (permalloy). The increase in damping with the thickness of the paramagnetic layer was interpreted as a result of spin pumping into the paramagnet. We determine the spin mixing conductance $g_{Pd}^{\uparrow\downarrow} = (3.8 \pm 0.5) \times 10^{18}$ m^{-2} at the FM–$Fe_{60}Al_{40}$/Pd interface and the spin diffusion length $\lambda_{Pd} = 9.1 \pm 2.0$ nm in Pd. For the PM–$Fe_{60}Al_{40}$/permalloy interface, we find a spin mixing conductance $g_{FeAl}^{\uparrow\downarrow} = (2.1 \pm 0.2) \times 10^{18}$ m^{-2} and a spin diffusion length $\lambda_{FeAl} = 11.9 \pm 0.2$ nm for PM–$Fe_{60}Al_{40}$. The demonstrated bi-functionality of the $Fe_{60}Al_{40}$ alloy in spin pumping structures may be promising for spintronic applications.

I. INTRODUCTION

Electronic devices based on utilization of spin currents represent a new generation of energy-efficient technology for ultrafast data processing. So-called pure spin currents (i.e., without the associated flow of electric charge in the circuit) can be produced via spin pumping—a transfer of angular momentum from a ferromagnetic layer to a metallic para- or diamagnet (PM, DM), often referred to as "normal" or "non-magnetic" metal—by microwave excitation of magnetization precession in the ferromagnet (FM). The latter is called ferromagnetic resonance (FMR).[1–5] Induced spin currents can be detected by the conversion to charge currents via the inverse spin Hall effect[6] as well as via FMR.[3,4,7–10] In the latter case, spin pumping is associated with the flow of spin angular momentum, which increases the spin relaxation rate and enhances the effective damping in the FM film.[3,4,9–13]

Characteristic quantities to estimate the spin pumping efficiency at FM/PM interfaces are the spin mixing conductance $g^{\uparrow\downarrow}$ and the spin diffusion length λ_{sd}. The former describes an interfacial dependent parameter of angular momentum transfer across the FM/PM interface. The latter describes the length scale of decay of the injected spin-current density into the adjacent non-ferromagnetic layer due to spin diffusion and relaxation.[14]

Both insulating [$Y_3Fe_5O_{12}$ (YIG), $Tm_3Fe_5O_{12}$ (TmIG)][15–17] and metallic ferromagnets (e.g., permalloy Py, Fe, Co, CoFeB, and FeRh)[18–23] have been used as spin sources, whereas metals with strong spin–orbit coupling[10,24–26] are usually used as spin-sink

layers. Important to note hybrid structures where both spin source and spin detector are made of ferromagnetic materials,[27,28] e.g., a spin current was injected from YIG into Py via a thermal gradient.[29] The interfacial spin transport was investigated with various types of non-ferromagnetic layers—such as semiconductors,[30,31] Rashba interfaces,[32] and topological insulators.[33–35] Recently, the focus has been extended to paramagnetic alloys,[7,36,37] which joined the family of confirmed spin sink materials inducing spin–orbit torque.

Here, we utilize the magnetostructural phase transition in the 3d metal binary alloy $Fe_{60}Al_{40}$ (FeAl) whose magnetic properties can be tuned via the change of the structural order[38–43] and investigate the dual role of a thin $Fe_{60}Al_{40}$ film as a spin source and a spin sink. $Fe_{60}Al_{40}$ alloy is known to form a B2-ordered intermetallic phase (CsCl-type) in thermal equilibrium,[44] which is paramagnetic at room temperature. Chemical disorder of the structure, i.e., formation of antisite defects, induces ferromagnetism associated with the increase in Fe–Fe nearest neighbors in an A2 structure and a lattice expansion.[42]

Structural disorder can be achieved during the deposition of thin films at room temperature without subsequent annealing. *In situ* annealing of sputtered films leads to formation of B2-ordered state which is paramagnetic at room temperature. B2-FeAl can be "switched" to the ferromagnetic state using mechanical deformation,[45] ion irradiation,[38,40] or fs laser pulses.[46] The laser-driven structural order–disorder transition allows for reversible writing and erasing of ferromagnetic regions in thin films.[46] Thus, taking advantage of the disorder-induced magnetization in FeAl, we address room temperature interfacial spin pumping in bilayer structures where, depending on its chemical structure, the FeAl thin film is implemented as ferromagnetic layer (spin source) or as paramagnetic layer (spin sink) and interfaced with two other metals commonly used for spin pumping experiments—Pd and permalloy $Ni_{80}Fe_{20}$. In the following, we define the ferromagnetic state of $Fe_{60}Al_{40}$ as spin source, emitting into an adjacent layer, and the paramagnetic state of $Fe_{60}Al_{40}$ as spin sink into which a spin current is pumped from a ferromagnetic material. We perform FMR measurements on a series of samples with different thickness of the PM layer, investigate an increase of the damping constant due to spin pumping, and determine the spin mixing conductance and the spin diffusion length for FM–$Fe_{60}Al_{40}$/Pd and PM–$Fe_{60}Al_{40}$/Py bilayers.

II. EXPERIMENT

The polycrystalline $Fe_{60}Al_{40}$, Py, and Pd films were sputter-deposited from alloy and elemental targets, respectively, onto a Si (100) substrate with a 250-nm-thick amorphous SiO_2 buffer layer. The chamber base pressure was $p = 2 \times 10^{-9}$ mbar (2×10^{-9} hPa). The magnetron sputtering was performed at room temperature in argon atmosphere of 3×10^{-3} mbar. The $Fe_{60}Al_{40}$ thin films deposited at room temperature have a chemically disordered A2 structure, which is ferromagnetic. Post-annealing *in situ* at 500 °C for 1h leads to the chemically ordered, non-ferromagnetic B2 structural phase.[42] Two sets of thin film bilayer samples have been investigated: (i) ferromagnetic 5-nm-thin A2-$Fe_{60}Al_{40}$ films capped with 2–10 nm Pd films, which were deposited at room temperature directly after FeAl deposition and (ii) 5-nm-thin Py films grown on top of an annealed paramagnetic B2-$Fe_{60}Al_{40}$ film of 5–20 nm thickness (see Fig. 1). In the latter case, the Py films have been deposited after *in situ* annealing of the FeAl films. Single 5-nm-thick FM A2-FeAl and Py films grown on Si/SiO_2 were used as a reference.

The broadband FMR measurements were performed at room temperature in the frequency range of 5–35 GHz. The samples were placed flip-chip on the center of a coplanar waveguide (CPW) connected to a Vector Network Analyzer (VNA, Agilent). By applying a microwave excitation on the sample, the amplitude and phase of CPW transmission signal is detected, which is usually called the complex scattering parameter S_{21}. The S_{21} parameter was recorded at a fixed frequency as a function of the magnetic field applied in in-plane as well as out-of-plane direction. By fitting each spectrum with a complex Lorentzian function,[47] the resonance field positions B_{res} and the peak-to-peak linewidth ΔB_{pp} values were determined and analyzed in terms of g-factor, effective magnetization, and damping parameter. To resolve the spin pumping contribution, we determined the frequency-dependent linewidth measured in an out-of-plane magnetic field in order to exclude the non-linear contributions to the linewidth such as two-magnon scattering and

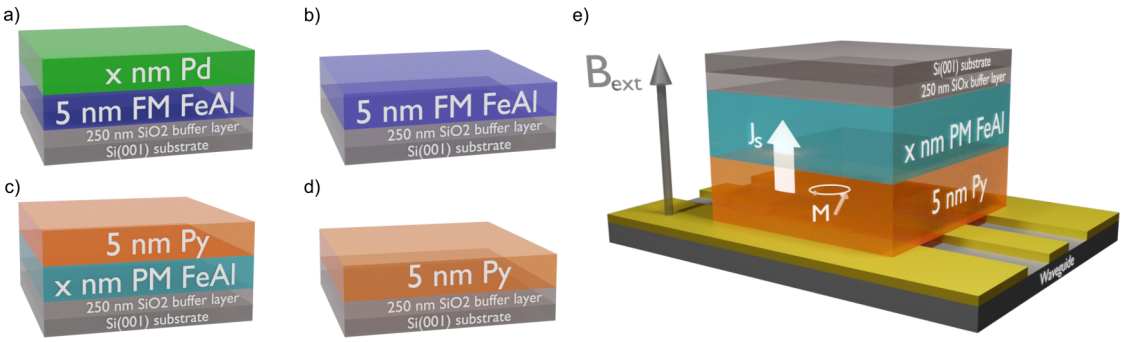

FIG. 1. Schematic representation of the investigated samples: (a) 5 nm thick ferromagnetic A2-disordered $Fe_{60}Al_{40}$ films capped with a Pd film of x = 2–10 nm thickness; (b) uncapped 5 nm A2-$Fe_{60}Al_{40}$ reference sample; (c) 5 nm Py films grown on top of paramagnetic B2-ordered $Fe_{60}Al_{40}$ film of thickness x = 5–20 nm; (d) 5 nm Py reference sample grown directly on Si/SiO_x substrate; (e) schematic of the VNA-FMR setup showing the coplanar waveguide and thin film sample in an out-of-plane applied static magnetic field for measuring a transmitted signal S_{21}.

mosaicity.[48] The dissipation and related broadening of linewidth due to eddy currents was neglected since the film thickness was smaller than the skin depth at FMR frequencies.

Static magnetic properties have been investigated using a Quantum Design MPMS system by recording $M(H)$ hysteresis loops at room temperature, which were normalized with respect to the volume of the ferromagnetic film.

III. RESULTS AND DISCUSSION

Figures 2(a) and 2(b) exemplary show out-of-plane FMR spectra measured at a frequency of 9.5 GHz for the two sample sets as sketched in Fig. 1. Figure 2(a) shows the spectrum of the uncapped as-grown 5 nm FM A2-FeAl film (blue line) and the one with 10 nm Pd cap layer (red). Figure 2(b) presents spectra of the single 5 nm Py film (blue) and a bilayer of 10 nm PM B2-FeAl/5 nm Py (red). One can observe an opposite shift of the resonance position and a change of the linewidth for the series based on FM and PM FeAl, which might be counterintuitive at the first glance but will be explained later on.

The resonance field as a function of the microwave frequency f in the out-of-plane geometry without cubic anisotropy is given by the Kittel equation[49,50]

$$B_{res}^{\perp}(f) = \frac{2\pi f}{|\gamma|} + \mu_0 M_{eff}, \tag{1}$$

where $\gamma = (g\mu_B)/\hbar$ is the gyromagnetic ratio, g is the Landé g-factor, μ_B is the Bohr magneton, and $\hbar$ is the reduced Planck constant. The effective magnetization is given by $\mu_0 M_{eff} = \mu_0 M_S - \mu_0 H_k$, where M_S is the saturation magnetization and $\mu_0 H_k = 2K_{2\perp}/M_S$ is the perpendicular anisotropy field with $K_{2\perp}$ being the perpendicular uniaxial magnetic anisotropy constant (often denoted as K_u). The g-factor and the effective magnetization values were extracted by fitting the experimental frequency dependence of the resonance field B_{res} according to Eq. (1) for each sample. The damping parameter α was evaluated from the frequency dependence of the linewidth ΔB_{pp} using the experimentally determined g-factor and the following relation:

$$\Delta B_{pp}(f) = \frac{4\pi\alpha}{\sqrt{3}|\gamma|} f + \Delta B_0, \tag{2}$$

where ΔB_0 is the frequency-independent inhomogeneous broadening due to structural and magnetic inhomogeneities of the sample.

Using reference measurements of the FM layers only, i.e., without adjacent spin-sink layers, the intrinsic Gilbert damping α_{int} and the spin-pumping contribution can be separated.[51] Thus, the total damping is given by[10,25,52]

$$\alpha = \alpha_{int} + g\mu_B \frac{g^{\uparrow\downarrow}}{4\pi M_S} \frac{1}{t_{FM}} \left(1 - e^{-\frac{2t_{PM}}{\lambda_{PM}}}\right), \tag{3}$$

where $g^{\uparrow\downarrow}$ denotes the spin mixing conductance of the FM/PM interface, t_{FM} and t_{PM} are the FM's and PM's thickness, respectively, and λ_{PM} is the spin diffusion length of the PM. The term in brackets accounts for a partial backflow of spin current at the interface, which depends on the thickness and the spin diffusion length of the adjacent layer.[10] We used the following values of saturation magnetization obtained from magnetometry at room temperature: $M_S = 650 \pm 70$ kA/m for 5 nm FM–$Fe_{60}Al_{40}$ and 690 ± 50 kA/m for 5 nm Py, similar to the ones reported earlier.[53,54]

The reference measurements revealed intrinsic Gilbert damping parameters α_{int} of $(5.04 \pm 0.11) \times 10^{-3}$ for 5 nm FM–$Fe_{60}Al_{40}$ and $(8.53 \pm 0.15) \times 10^{-3}$ for the 5 nm Py thin film. The damping parameter of the thin Py layer is in good agreement with the previously reported values of 8.5×10^{-3} for 7 nm thickness.[31]

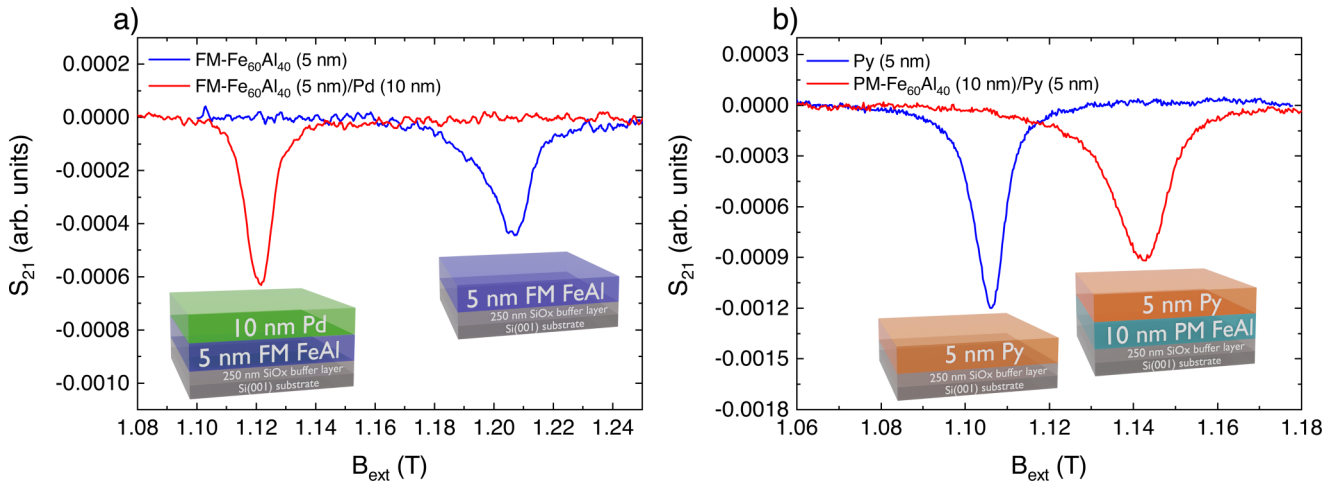

FIG. 2. (a) FMR spectra of the 5-nm-thick ferromagnetic A2-$Fe_{60}Al_{40}$ film: uncapped (blue) and capped with 10 nm Pd (red); (b) FMR spectra of 5-nm-thick Py films: single (blue) and bilayer with 10 nm paramagnetic B2-$Fe_{60}Al_{40}$ (red). All spectra were measured in the magnetic field applied in the out-of-plane direction at a frequency of 9.500 GHz and room temperature.

A. A2-disordered ferromagnetic $Fe_{60}Al_{40}$ as a spin source

First, spin pumping in the bilayer system FM–FeAl/Pd [Figs. 1(a) and 1(b)] was studied to determine the spin diffusion length of Pd and the spin mixing conductance at the interface with as-grown A2-FeAl. Figures 3(a) and 3(b) show the frequency dependence of the resonance field B_{res} and the linewidth ΔB_{pp} of the uncapped 5 nm thick FM−FeAl film and of the films capped with a 2, 3, 5, and 10 nm Pd layer. The g-factor and the effective magnetization [Figs. 3(c) and 3(d)] have been extracted by fitting the data according to Eq. (1). The g-factor of the single FM−FeAl film is 2.042 ± 0.002, while for Pd-capped films it increases by 0.3% to 2.048 ± 0.002, remaining independent of the Pd thickness within the error bar. This increase is related to the change in the ratio of the effective spin to orbital magnetic moment due to Pd capping.[55,56] Also, the polarization of Pd at the interface may play a role—similarly to the observations in Fe/V superlattices.[57]

This interpretation is supported by the observed decrease in the effective magnetization [Fig. 3(d)] most likely due to a change in the magneto-crystalline anisotropy.[58] Additionally, on the surface of non-capped FM–FeAl, a self-passivating oxide layer is formed, which affects the contribution of the surface anisotropy to the effective magnetization [Fig. 3(d)], seen as a shift of the resonance field for the uncapped film in Fig. 3(a). Based on the FMR and magnetometry data, we determined the anisotropy field $2K_{2\perp}/M_s$ of −61 ± 7 mT for uncapped 5 nm FM–FeAl films and 34 ± 4 mT for Pd-capped films, which is similar to the values reported in our previous work on 40 nm FM–FeAl films, where ferromagnetic ordering has been introduced via neon ion irradiation with the energy 17.5–30 keV.[40]

The ferromagnetic resonance peak-to-peak linewidth ΔB_{pp} vs frequency [Fig. 3(b)] fitted accordingly to Eq. (2) reveals an inhomogeneous broadening of 6.1 ± 0.4 mT for the uncapped film and of 2.4 ± 0.5 mT for all capped films [Fig. 3(e)]. This explains why the linewidth of the uncapped FM–FeAl film in Fig. 2(a) was counterintuitively larger than the one with the spin sink on top. After subtraction of the inhomogeneous line broadening, an increase in the linear slope (corresponding to α) as a function of the capping layer thickness caused by the spin pumping can be seen. This increase in the Gilbert-like damping α is shown in Fig. 4 in detail. The spin mixing conductance $g_{Pd}^{\uparrow\downarrow} = (3.8 \pm 0.5) \times 10^{18}$ m^{-2} of the FM–$Fe_{60}Al_{40}$/Pd bilayer and the spin diffusion length $\lambda_{Pd} = 9.1 \pm 2$ nm of Pd was evaluated from the dependence of α as a function of Pd thickness t_{Pd} according to Eq. (3). The possible error in evaluation of saturation magnetization (passivating layer, inaccuracy in the evaluation of the FM layer volume) is accounted for by giving a larger error bar for $g_{Pd}^{\uparrow\downarrow}$.[59]

The spin diffusion lengths of Pd reported in the literature, e.g., $\lambda_{Pd} = 8.6 \pm 1$ nm for $Co_{90}Fe_{10}(2)$/Pd[60] are within the error bar of our measurement. Previously reported values for the spin mixing

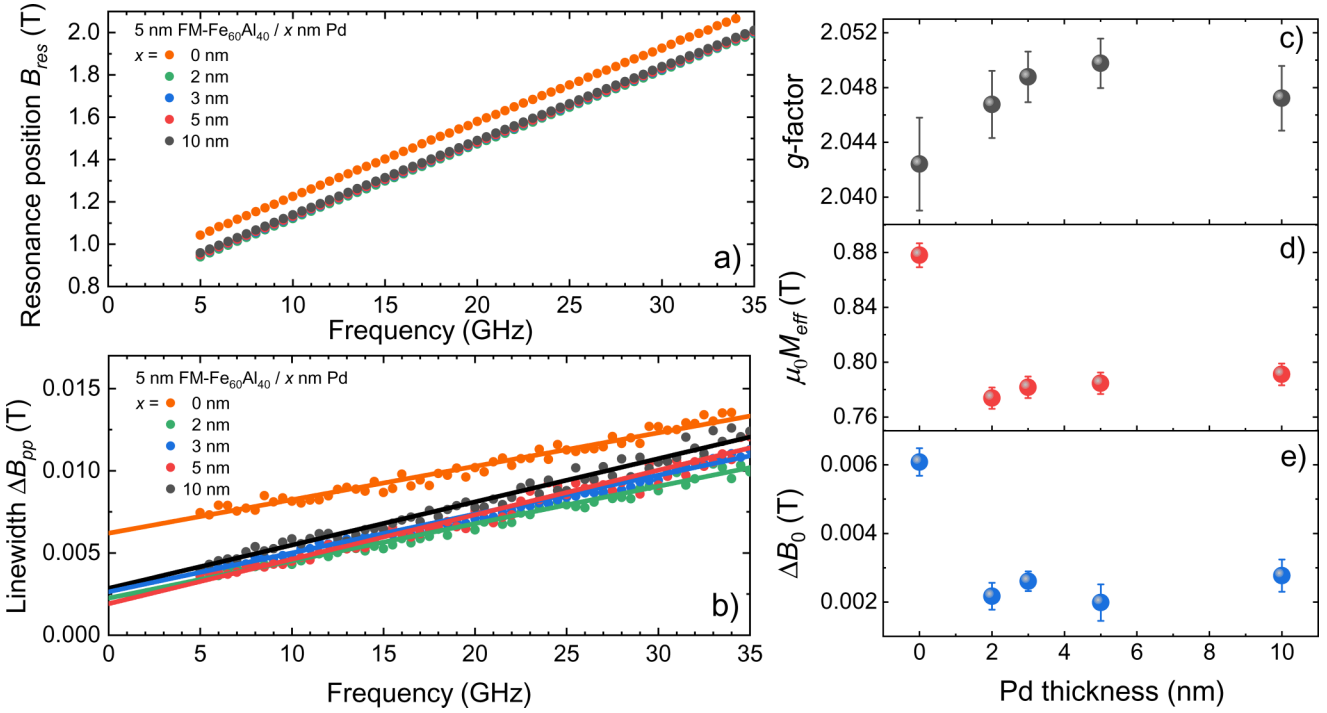

FIG. 3. (a) Resonance position as a function of frequency at room temperature, (b) frequency-dependent linewidth (symbols) and linear fit (solid line) according to Eq. (2) for different Pd thickness on top of the 5 nm FM A2-$Fe_{60}Al_{40}$ thin film, (c) g-factor, (d) effective magnetization $\mu_0 M_{eff}$, and (e) inhomogeneous broadening ΔB_0 of 5 nm FM A2-$Fe_{60}Al_{40}$/Pd as a function of Pd layer thickness.

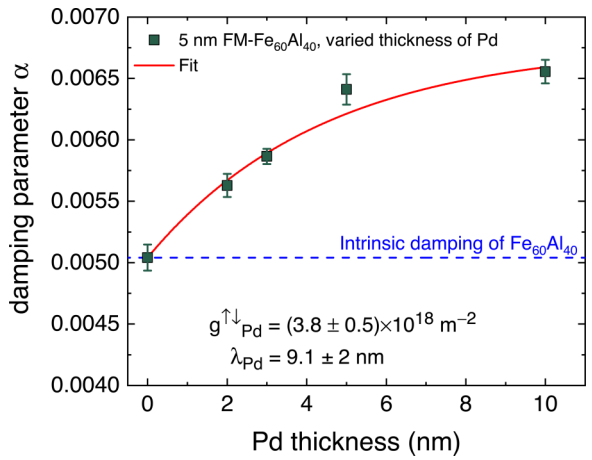

FIG. 4. Damping parameter α of 5 nm FM A2-$Fe_{60}Al_{40}$ films in dependence of the Pd capping layer thickness. The solid red line indicates the fit according to Eq. (3). The dashed blue line shows the intrinsic damping contribution of the ferromagnetic $Fe_{60}Al_{40}$ layer without capping.

conductance at Pd interfaces with different FM films are ranging significantly due to varying interface conditions like the crystallinity of the FM layer,[61] the chemical composition,[60] and the morphology of the interface[62] as well as due to varied detection methods. The obtained spin mixing conductance of the FM–FeAl/Pd interface is comparable to the reported value for Fe/Pd.[52] A broad variation within the published values of $g^{\uparrow\downarrow}_{Pd}$ in case of Fe/Pd as well as Py/Pd interfaces might also be ascribed to the alloying and the change of interface roughness in capped films. Our study shows that an A2-disordered FM–FeAl alloy can generate a spin pumping into an adjacent paramagnetic layer, which is confirmed by FMR and the determination of the spin-diffusion length of Pd.

B. B2-ordered paramagnetic $Fe_{60}Al_{40}$ as a spin sink

Our next step was to investigate spin pumping in thin film bilayers where $Fe_{60}Al_{40}$ is used in its B2-ordered paramagnetic state as a spin sink [Fig. 1(c)]. FMR measurements as described above were performed on the series of 5 nm thin Py films grown on top of the paramagnetic B2-FeAl films of varied thickness as summarized in Fig. 5. Based on the analysis of the resonance field and frequency [Fig. 5(a)] using Eqs. (1) and (2), the values of g-factor and M_{eff} of the Py films with and without PM–FeAl layer were found [Figs. 5(c) and 5(d)].

The g-factor for the single Py film grown directly on a Si/SiO_x substrate is $g = 2.098 \pm 0.001$, which is in good agreement with the value reported by Shaw *et al.*, who showed that the g-factor of Py for the out-of-plane geometry is decreasing with the reciprocal thickness, leading to a smaller g-factor than the bulk value of $g^{bulk}_{Py} = 2.109 \pm 0.003$.[63]

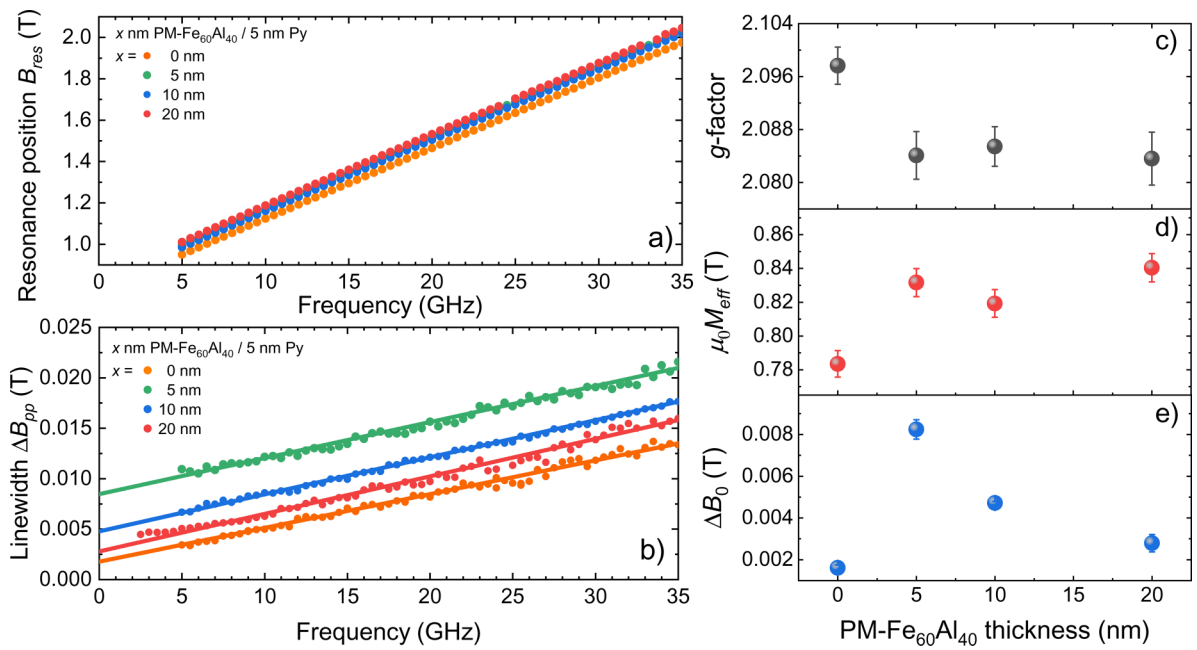

FIG. 5. (a) Resonance position as a function of frequency at room temperature, (b) frequency-dependent linewidth (symbols) of 5 nm Py and linear fit (solid line) according to Eq. (2) for different thickness of the underlying PM–$Fe_{60}Al_{40}$ layers, (c) g-factor, (d) effective magnetization $\mu_0 M_{eff}$, and (e) inhomogeneous broadening ΔB_0 as a function of the B2-ordered PM–$Fe_{60}Al_{40}$ underlayer thickness.

When a Py film is deposited on top of the B2-ordered PM–FeAl, the g-factor decreases to $g = 2.084 \pm 0.002$ and remains constant within the error bar for the presented FeAl layer thickness range [Fig. 5(c)]. In contrast, the effective magnetization of the Py film was found to be higher for the bilayer samples reaching the value of 0.83 ± 0.01 T while for single Py layer it was 0.78 ± 0.01 T. Both these values are reduced in comparison to the bulk permalloy saturation magnetization ($\mu_0 M_S^{Py\ bulk} = 1$ T) and obtained here for 5 nm Py film ($\mu_0 M_S^{Py\ 5\ nm} = 0.867$ T), which implies a positive perpendicular magnetic anisotropy field $2K_{2\perp}/M_s$ known for thin films.[64,65] The perpendicular magnetic anisotropy is decreasing for the PM–FeAl/Py bilayer in comparison to single Py films, which is also consistent with a decrease in the g-factor. We assume this reversed effect of an adjacent PM layer on the g-factor [Fig. 5(c)] and effective magnetization [Fig. 5(d)] in contrast to the FM–FeAl/Pd bilayers [Figs. 3(c) and 3(d)] is due to the increase in the ratio of spin-to-orbital magnetic moment.

The analysis of the peak-to-peak linewidth ΔB_{pp} vs frequency [Fig. 5(b)] fitted to Eq. (2) reveals an inhomogeneous broadening of 1.6 ± 0.1 mT for the single 5 nm Py film grown on Si/SiO_x and 8.2 to 2.8 ± 0.5 mT for the 5 nm Py films grown on top of PM–FeAl, prominently decreasing with FeAl thickness [Fig. 5(e)], which might be associated with the improved surface roughness of the thicker films. After subtraction of the inhomogeneous broadening, the increase of the linear slope with increasing thickness of the PM–FeAl interfaced with the Py film is evident (Fig. 6). Both parameters $g_{FeAl}^{\uparrow\downarrow}$ of the PM B2-FeAl/Py interface and λ_{FeAl} of PM–FeAl were determined. According to Eq. (3), one obtains $g_{FeAl}^{\uparrow\downarrow} = (2.1 \pm 0.2) \times 10^{18}$ m^{-2} and $\lambda_{FeAl} = 11.9 \pm 0.2$ nm.

When interfaced with Py, PM–$Fe_{60}Al_{40}$ exhibits an almost 31% larger spin diffusion length as compared to Pd, which is consistent with the smaller spin–orbit coupling in the PM–$Fe_{60}Al_{40}$ alloy. The spin mixing conductance of PM–FeAl/Py is smaller as compared to the FM–FeAl/Pd interface. Since the formation of an interfacial oxide layer between PM–FeAl and Py during deposition is excluded, we attribute the determined value $g_{FeAl}^{\uparrow\downarrow}$ to intrinsic properties of the interface, as described above. A significant variation of the inhomogeneous broadening of the Py resonance line depending on the thickness of the underlying PM–FeAl layer might indicate a non-vanishing role of surface roughness, which in turn affects the transparency of the interface for the spin current.[62] Currently, we conclude that the $Fe_{60}Al_{40}$ alloy in a paramagnetic B2-ordered state can be used as spin sink in spin pumping experiments.

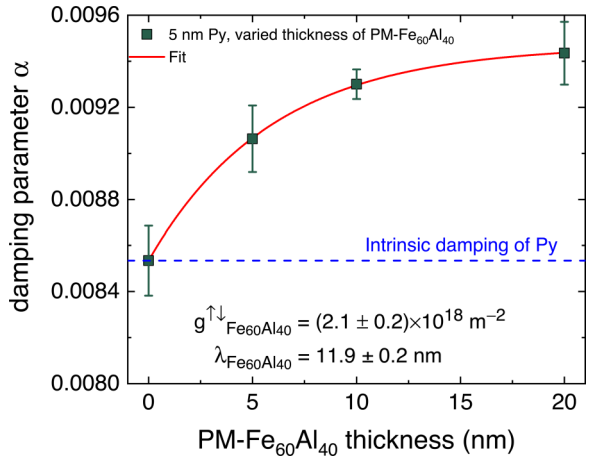

FIG. 6. Extracted damping parameter α of 5 nm Py films depending on the thickness of the PM–$Fe_{60}Al_{40}$ layer. The solid red line indicates the fit to Eq. (3). The dashed blue line shows the intrinsic damping contribution of the 5 nm Py thin film.

Summarizing, spin pumping experiments performed on two sets of bilayer samples, i.e., FM–FeAl/Pd and PM–FeAl/Py with an identical chemical composition of $Fe_{60}Al_{40}$, demonstrate the bi-functionality of this alloy in spintronics and show that it can be used as a spin source and spin sink at room temperature depending on its structural order. Engineering an interface design, e.g., by combining FM–$Fe_{60}Al_{40}$ and PM–$Fe_{60}Al_{40}$ as a bilayer as well as laterally patterned nanostructures by ion-beam[41] or laser irradiation,[46] might be a promising approach to generate pure spin currents via spin pumping.

IV. CONCLUSIONS

The spin pumping efficiency of the $Fe_{60}Al_{40}$ alloy in bilayer systems acting as a spin source and as a spin sink when formed in A2/B2 structural order has been studied using FMR. $Fe_{60}Al_{40}$ layers were prepared in the A2-disordered ferromagnetic state and in the B2-ordered paramagnetic state and interfaced with thin films of Pd and Py ($Ni_{80}Fe_{20}$), respectively. We determined the spin mixing conductance $g_{Pd}^{\uparrow\downarrow} = (3.8 \pm 0.5) \times 10^{18}$ m^{-2} of the FM–$Fe_{60}Al_{40}$/Pd interface and the spin diffusion length $\lambda_{Pd} = 9.1 \pm 2$ nm in Pd as well as the spin mixing conductance $g_{FeAl}^{\uparrow\downarrow} = (2.1 \pm 0.2) \times 10^{18}$ m^{-2} of the PM–$Fe_{60}Al_{40}$/Py interface and the spin diffusion length $\lambda_{FeAl} = 11.9 \pm 0.2$ nm in PM–$Fe_{60}Al_{40}$. The possibility to use $Fe_{60}Al_{40}$ thin films of the same chemical composition at room temperature as spin sink and spin source may add an additional degree of freedom in the design of spintronic and magnonic devices based on the generation, manipulation, and detection of pure spin currents.

ACKNOWLEDGMENTS

We acknowledge the funding by the German Research Foundation (DFG, Deutsche Forschungsgemeinschaft) within Project No. 392402498 (SE 2853/1-1|AL 618/37-1) and partial funding within Collaborative Research Centre/Transregio (CRC/TRR) 270, project A04 (Project No. 405553726). R.B. acknowledges funding by the DFG within Project No. 322462997 (BA 5656/1-2|WE 2623/14-2). We thank Professor B. Aktas for helpful discussions.

AUTHOR DECLARATIONS

Conflict of Interest

The authors have no conflicts to disclose.

Author Contributions

T. Strusch: Investigation (equal); Visualization (lead); Writing – original draft (lead); Writing – review & editing (equal). **K. Lenz:** Formal analysis (supporting); Investigation (supporting); Methodology (equal); Software (lead); Writing – review & editing (equal). **R. Meckenstock:** Writing – review & editing (equal). **R. Bali:** Writing – review & editing (equal). **J. Ehrler:** Methodology (equal). **J. Lindner:** Writing – review & editing (equal). **J. Fassbender:** Project administration (supporting). **M. Farle:** Supervision (equal); Writing – review & editing (equal). **K. Potzger:** Methodology (equal); Project administration (supporting); Writing – review & editing (equal). **A. Semisalova:** Funding acquisition (lead); Investigation (equal); Project administration (lead); Supervision (lead); Writing – original draft (equal); Writing – review & editing (equal).

DATA AVAILABILITY

The data that support the findings of this study are available from the corresponding author upon reasonable request.

REFERENCES

[1]Y. Tserkovnyak, A. Brataas, and G. E. W. Bauer, "Spin pumping and magnetization dynamics in metallic multilayers," Phys. Rev. B **66**, 224403 (2002).
[2]Y. Tserkovnyak, A. Brataas, and G. E. W. Bauer, "Enhanced Gilbert damping in thin ferromagnetic films," Phys. Rev. Lett. **88**, 117601(4) (2002).
[3]B. Heinrich, Y. Tserkovnyak, G. Woltersdorf, A. Brataas, R. Urban, and G. E. W. Bauer, "Dynamic exchange coupling in magnetic bilayers," Phys. Rev. Lett. **90**, 187601 (2003).
[4]R. Urban, B. Heinrich, and G. Woltersdorf, "Semiclassical theory of spin transport in magnetic multilayers," J. Appl. Phys. **93**, 8280 (2003).
[5]M. Belmeguenai, M. S. Gabor, F. Zighem, N. Challab, T. Petrisor, R. B. Mos, and C. Tiusan, "Ferromagnetic-resonance-induced spin pumping in $Co_{20}Fe_{60}B_{20}$/Pt systems: Damping investigation," J. Phys. D: Appl. Phys. **51**, 045002 (2018).
[6]S. R. Boona, R. C. Myers, and J. P. Heremans, "Spin caloritronics," Energy Environ. Sci. **7**, 885 (2014).
[7]M. W. Keller, K. S. Gerace, M. Arora, E. K. Delczeg-Czirjak, J. M. Shaw, and T. J. Silva, "Near-unity spin Hall ratio in Ni_xCu_{1-x} alloys," Phys. Rev. B **99**, 214411 (2019).
[8]M. Belmeguenai, K. Aitoukaci, F. Zighem, M. S. Gabor, T. Petrisor, R. B. Mos, and C. Tiusan, "Investigation of the annealing temperature dependence of the spin pumping in $Co_{20}Fe_{60}B_{20}$/Pt systems," J. Appl. Phys. **123**, 113905 (2018).
[9]M. Charilaou, K. Lenz, and W. Kuch, "Spin-pumping-enhanced magnetic damping in ultrathin Cu(001)/Co/Cu and Cu(001)/Ni/Cu films," J. Magn. Magn. Mater. **322**, 2065 (2010).
[10]J. M. Shaw, H. T. Nembach, and T. J. Silva, "Determination of spin pumping as a source of linewidth in sputtered Co90Fe10/Pd multilayers by use of broadband ferromagnetic resonance spectroscopy," Phys. Rev. B: Condens. Matter Mater. Phys. **85**, 054412(10) (2012).
[11]Y. Li, W. Zhang, N. Li, R. Sun, J. Tang, Z. Z. Gong, Y. Li, X. Yang, Z. K. Xie, Q. Gul, X. Q. Zhang, W. He, and Z. H. Cheng, "Optical determination of spin diffusion length and interfacial spin mixing conductance in epitaxial Pd/Fe bilayers," J. Phys.: Condens. Matter **31**, 305802 (2019).
[12]M. Zwierzycki, Y. Tserkovnyak, P. J. Kelly, A. Brataas, and G. E. W. Bauer, "First-Principles study of magnetization relaxation enhancement and spin transfer in thin magnetic films," Phys. Rev. B **71**, 064420 (2005).
[13]I. Barsukov, H. K. Lee, A. A. Jara, Y. J. Chen, A. M. Gonçalves, C. Sha, J. A. Katine, R. E. Arias, B. A. Ivanov, and I. N. Krivorotov, "Giant nonlinear damping in nanoscale ferromagnets," Sci. Adv. **5**, eaav6943 (2019).
[14]A. Azevedo, L. H. Vilela-Leao, R. L. Rodriguez-Suarez, A. F. Lacerda Santos, and S. M. Rezende, "Spin pumping and anisotropic magnetoresistance voltages in magnetic bilayers: Theory and experiment," Phys. Rev. B **83**, 144402 (2011).
[15]B. Heinrich, C. Burrowes, E. Montoya, B. Kardasz, E. Girt, Y. Y. Song, Y. Sun, and M. Wu, "Spin pumping at the magnetic insulator (YIG)/normal metal (Au) interfaces," Phys. Rev. Lett. **107**, 066604 (2011).
[16]H. L. Wang, C. H. Du, Y. Pu, R. Adur, P. C. Hammel, and F. Y. Yang, "Large spin pumping from epitaxial Y3Fe5O12 thin films to Pt and W layers," Phys. Rev. B **88**, 100406(R) (2013).
[17]A. Quindeau, C. O. Avci, W. Liu, C. Sun, M. Mann, A. S. Tang, M. C. Onbasli, D. Bono, P. M. Voyles, Y. Xu, J. Robinson, G. S. D. Beach, and C. A. Ross, "Tm3fe5o12/Pt heterostructures with perpendicular magnetic anisotropy for spintronic applications," Adv. Electron. Mater. **3**, 1600376 (2017).
[18]O. Mosendz, V. Vlaminck, J. E. Pearson, F. Y. Fradin, G. E. W. Bauer, S. D. Bader, and A. Hoffmann, "Detection and quantification of inverse spin Hall effect from spin pumping in permalloy/Normal metal bilayers," Phys. Rev. B **82**, 214403 (2010).
[19]G. Woltersdorf, M. Buess, B. Heinrich, and C. H. Back, "Time resolved magnetization dynamics of ultrathin Fe(001) films: Spin-pumping and two-magnon scattering," Phys. Rev. Lett. **95**, 037401 (2005).
[20]T. G. A. Verhagen, H. N. Tinkey, H. C. Overweg, M. van Son, M. Huber, J. M. van Ruitenbeek, and J. Aarts, "Temperature dependence of spin pumping and gilbert damping in thin Co/Pt bilayers," J. Phys.: Condens. Matter **28**, 056004 (2016).
[21]A. Ruiz-Calaforra, T. Brächer, V. Lauer, P. Pirro, B. Heinz, M. Geilen, A. V. Chumak, A. Conca, B. Leven, and B. Hillebrands, "The role of the Non-magnetic material in spin pumping and magnetization dynamics in NiFe and CoFeB multilayer systems," J. Appl. Phys. **117**, 163901 (2015).
[22]K. Tanaka, T. Moriyama, T. Usami, T. Taniyama, and T. Ono, "Spin torque in FeRh alloy measured by spin-torque ferromagnetic resonance," Appl. Phys. Express **11**, 013008 (2018).
[23]Y. Wang, M. M. Decker, T. N. G. Meier, X. Chen, C. Song, T. Grünbaum, W. Zhao, J. Zhang, L. Chen, and C. H. Back, "Spin pumping during the antiferromagnetic–ferromagnetic phase transition of iron–rhodium," Nat. Commun. **11**, 275 (2020).
[24]C. Burrowes, B. Heinrich, B. Kardasz, E. A. Montoya, E. Girt, Y. Sun, Y.-Y. Song, and M. Wu, "Enhanced spin pumping at yttrium iron garnet/Au interfaces," Appl. Phys. Lett. **100**, 092403 (2012).
[25]A. Kumar, S. Akansel, H. Stopfel, M. Fazlali, J. Akerman, R. Brucas, and P. Svedlindh, "Spin transfer torque ferromagnetic resonance induced spin pumping in the Fe/Pd bilayer system," Phys. Rev. B **95**, 064406 (2017).
[26]M. Caminale, A. Ghosh, S. Auffret, U. Ebels, K. Ollefs, F. Wilhelm, A. Rogalev, and W. E. Bailey, "Spin pumping damping and magnetic proximity effect in Pd and Pt spin-sink layers," Phys. Rev. B **94**, 014414 (2016).
[27]H. Wang, C. Du, P. Chris Hammel, and F. Yang, "Spin current and inverse spin Hall effect in ferromagnetic metals probed by $Y_3Fe_5O_{12}$-based spin pumping," Appl. Phys. Lett. **104**, 202405 (2014).
[28]A. Azevedo, O. Alves Santos, G. A. Fonseca Guerra, R. O. Cunha, R. Rodríguez-Suárez, and S. M. Rezende, "Competing spin pumping effects in magnetic hybrid structures," Appl. Phys. Lett. **104**, 052402 (2014).
[29]B. F. Miao, S. Y. Huang, D. Qu, and C. L. Chien, "Inverse spin Hall effect in a ferromagnetic metal," Phys. Rev. Lett. **111**, 066602 (2013).
[30]K. Ando and E. Saitoh, "Observation of the inverse spin Hall effect in silicon," Nat. Commun. **3**, 629 (2012).
[31]R. Ohshima, S. Klingler, S. Dushenko, Y. Ando, M. Weiler, H. Huebl, T. Shinjo, S. T. B. Goennenwein, and M. Shiraishi, "Spin injection into silicon detected by broadband ferromagnetic resonance spectroscopy," Appl. Phys. Lett. **110**, 182402 (2017).
[32]K. Chen and S. Zhang, "Spin pumping in the presence of spin-orbit coupling," Phys. Rev. Lett. **114**, 126602 (2015).
[33]J. C. Rojas-Sanchez, S. Oyarzun, Y. Fu, A. Marty, C. Vergnaud, S. Gambarelli, L. Vila, M. Jamet, Y. Ohtsubo, A. Taleb-Ibrahimi, P. Le Fevre, F. Bertran,

N. Reyren, J. M. George, and A. Fert, "Spin to charge conversion at room temperature by spin pumping into a new type of topological insulator: A-Sn films," Phys. Rev. Lett. **116**, 096602 (2016).
[34]M. Jamali, J. S. Lee, J. S. Jeong, F. Mahfouzi, Y. Lv, Z. Zhao, B. K. Nikolić, K. A. Mkhoyan, N. Samarth, and J.-P. Wang, "Giant spin pumping and inverse spin Hall effect in the presence of surface and bulk spin−orbit coupling of topological insulator Bi_2Se_3," Nano Lett. **15**, 7126 (2015).
[35]A. Navabi, Y. Liu, P. Upadhyaya, K. Murata, F. Ebrahimi, G. Yu, B. Ma, Y. Rao, M. Yazdani, M. Montazeri, L. Pan, I. N. Krivorotov, I. Barsukov, Q. Yang, P. Khalili Amiri, Y. Tserkovnyak, and K. L. Wang, "Control of spin-wave damping in YIG using spin currents from topological insulators," Phys. Rev. Appl. **11**, 034046 (2019).
[36]Y. Hibino, T. Taniguchi, K. Yakushiji, A. Fukushima, H. Kubota, and S. Yuasa, "Large spin-orbit-torque efficiency generated by spin Hall effect in paramagnetic Co-Ni-B alloys," Phys. Rev. Appl. **14**, 064056 (2020).
[37]M. Li, L. Jin, Y. H. Rao, Z. Zhong, X. Tang, B. Liu, H. Meng, Q. Yang, Y. Lin, and H. Zhang, "Large spin Hall angle in nonmagnetic PtSn alloy films at room temperature," J. Magn. Magn. Mater. **507**, 166860 (2020).
[38]R. Bali, S. Wintz, F. Meutzner, R. Hübner, R. Boucher, A. A. Ünal, S. Valencia, A. Neudert, K. Potzger, J. Bauch, F. Kronast, S. Facsko, J. Lindner, and J. Fassbender, "Printing nearly-discrete magnetic patterns using chemical disorder induced ferromagnetism," Nano Lett. **14**, 435 (2014).
[39]F. Röder, G. Hlawacek, S. Wintz, R. Hübner, L. Bischoff, H. Lichte, K. Potzger, J. Lindner, J. Fassbender, and R. Bali, "Direct depth- and lateral-imaging of nanoscale magnets generated by ion impact," Sci. Rep. **5**, 16786 (2015).
[40]T. Schneider, K. Lenz, A. Semisalova, J. Gollwitzer, J. Heitler-Klevans, K. Potzger, J. Fassbender, J. Lindner, and R. Bali, "Tuning ferromagnetic resonance via disorder/order interfaces," J. Appl. Phys. **125**, 195302 (2019).
[41]M. Nord, A. Semisalova, A. Kákay, G. Hlawacek, I. MacLaren, V. Liersch, O. M. Volkov, D. Makarov, G. W. Paterson, K. Potzger, J. Lindner, J. Fassbender, D. McGrouther, and R. Bali, "Strain anisotropy and magnetic domains in embedded nanomagnets," Small **15**, 1904738 (2019).
[42]J. Ehrler, B. Sanyal, J. Grenzer, S. Zhou, R. Böttger, B. Eggert, H. Wende, J. Lindner, J. Fassbender, C. Leyens, K. Potzger, and R. Bali, "Magneto-structural correlations in a systematically disordered B2 lattice," New J. Phys. **22**, 073004 (2020).
[43]K. Borisov, J. Ehrler, C. Fowley, B. Eggert, H. Wende, S. Cornelius, K. Potzger, J. Lindner, J. Fassbender, R. Bali, and P. Stamenov, "Spin polarization and magnetotransport properties of systematically disordered $Fe_{60}Al_{40}$ thin films," Phys. Rev. B **104**, 134417 (2021).
[44]M. Palm, F. Stein, and G. Dehm, "Iron aluminides," Annu. Rev. Mater. Res. **49**, 297 (2019).
[45]E. Menéndez, J. Sort, M. O. Liedke, J. Fassbender, S. Suriñach, M. D. Baró, and J. Nogués, "Two-fold origin of the deformation-induced ferromagnetism in bulk Fe60Al40(at.%) alloys," New J. Phys. **10**, 103030 (2008).
[46]J. Ehrler, M. He, M. V. Shugaev, N. I. Polushkin, S. Wintz, V. Liersch, S. Cornelius, R. Hübner, K. Potzger, J. Lindner, J. Fassbender, A. A. Ünal, S. Valencia, F. Kronast, L. V. Zhigilei, and R. Bali, "Laser-rewriteable ferromagnetism at thin-film surfaces," ACS Appl. Mater. Interfaces **10**, 15232 (2018).
[47]M. O. Liedke, M. Körner, K. Lenz, M. Fritzsche, M. Ranjan, A. Keller, E. Čižmár, S. A. Zvyagin, S. Facsko, K. Potzger, J. Lindner, and J. Fassbender, "Crossover in the surface anisotropy contributions of ferromagnetic films on rippled Si surfaces," Phys. Rev. B **87**, 024424 (2013).
[48]K. Zakeri, J. Lindner, I. Barsukov, R. Meckenstock, M. Farle, U. von Hörsten, H. Wende, W. Keune, J. Rocker, S. S. Kalarickal, K. Lenz, W. Kuch, K. Baberschke, and Z. Frait, "Spin dynamics in ferromagnets: Gilbert damping and two-magnon scattering," Phys. Rev. B **76**, 104416 (2007).
[49]J. M. Shaw, H. T. Nembach, and T. J. Silva, "Measurement of orbital asymmetry and strain in Co90Fe 10/Ni multilayers and alloys: Origins of perpendicular anisotropy," Phys. Rev. B **87**, 054416 (2013).
[50]C. Kittel, "On the theory of ferromagnetic resonance absorption," Phys. Rev. **73**, 155 (1948).
[51]A. M. Gonçalves, F. Garcia, H. K. Lee, A. Smith, P. R. Soledade, C. A. C. Passos, M. Costa, N. M. Souza-Neto, I. N. Krivorotov, L. C. Sampaio, and I. Barsukov, "Oscillatory interlayer coupling in spin Hall systems," Sci. Rep. **8**, 2318 (2018).
[52]J. Foros, G. Woltersdorf, B. Heinrich, and A. Brataas, "Scattering of spin current injected in Pd(001)," J. Appl. Phys. **97**, 10A714 (2005).
[53]A. Hrabec, F. J. T. Gonçalves, C. S. Spencer, E. Arenholz, A. T. N'Diaye, R. L. Stamps, and C. H. Marrows, "Spin-Orbit interaction enhancement in permalloy thin films by Pt doping," Phys. Rev. B **93**, 014432 (2016).
[54]S. Martín-Rio, A. Pomar, L. Balcells, B. Bozzo, C. Frontera, and B. Martínez, "Temperature dependence of spin pumping and inverse spin Hall effect in permalloy/Pt bilayers," J. Magn. Magn. Mater. **500**, 166319 (2020).
[55]C. Le Graët, D. Spenato, N. Beaulieu, D. T. Dekadjevi, J.-P. Jay, S. P. Pogossian, B. Warot-Fonrose, and J. Ben Youssef, "Driving mechanism for damping and G-factor in Non-amorphous ferromagnetic CoFeZr ultrathin films," Europhys. Lett. **115**, 17002 (2016).
[56]F. Schreiber, J. Pflaum, Z. Frait, T. Mühge, and J. Pelzl, "Gilbert damping and G-factor in FexCo1−x alloy films," Solid State Commun. **93**, 965 (1995).
[57]A. N. Anisimov, M. Farle, P. Poulopoulos, W. Platow, K. Baberschke, P. Isberg, R. Wäppling, A. M. N. Niklasson, and O. Eriksson, "Orbital magnetism and magnetic anisotropy probed with ferromagnetic resonance," Phys. Rev. Lett. **82**, 2390 (1999).
[58]S. Mizukami, Y. Ando, and T. Miyazaki, "The study on ferromagnetic resonance linewidth for NM/80NiFe/NM (NM = Cu, Ta, Pd and Pt) films," Jpn. J. Appl. Phys. **40**, 580 (2001).
[59]Q. Liu, X. Chen, J. Y. Zhang, M. Yang, X. J. Li, S. L. Jiang, Y. W. Liu, Y. Cao, Z. L. Wu, C. Feng, L. Ding, and G. H. Yu, "Effects of interfacial Fe electronic structures on magnetic and electronic transport properties in oxide/NiFe/oxide heterostructures," Appl. Surf. Sci. **349**, 524 (2015).
[60]M. B. Jungfleisch, V. Lauer, R. Neb, A. V. Chumak, and B. Hillebrands, "Improvement of the yttrium iron garnet/platinum interface for spin pumping-based applications," Appl. Phys. Lett. **103**, 022411 (2013).
[61]Z. Qiu, K. Ando, K. Uchida, Y. Kajiwara, R. Takahashi, H. Nakayama, T. An, Y. Fujikawa, and E. Saitoh, "Spin mixing conductance at a well-controlled platinum/yttrium iron garnet interface," Appl. Phys. Lett. **103**, 092404 (2013).
[62]E. T. Papaioannou, P. Fuhrmann, M. B. Jungfleisch, T. Brächer, P. Pirro, V. Lauer, J. Lösch, and B. Hillebrands, "Optimizing the spin-pumping induced inverse spin Hall voltage by crystal growth in Fe/Pt bilayers," Appl. Phys. Lett. **103**, 162401 (2013).
[63]J. M. Shaw, H. T. Nembach, T. J. Silva, and C. T. Boone, "Precise determination of the spectroscopic G-factor by use of broadband ferromagnetic resonance spectroscopy," J. Appl. Phys. **114**, 243906 (2013).
[64]S. Karimeddiny and D. C. Ralph, "Resolving discrepancies in spin-torque ferromagnetic resonance measurements: Lineshape versus linewidth analyses," Phys. Rev. Appl. **15**, 064017 (2021).
[65]B. Bhagat, A. Semisalova, R. Meckenstock, and M. Farle, "Reversal of uniaxial magnetic anisotropy in Fe/GaAs (110) films driven by surface relaxation: An *in situ* ferromagnetic resonance study," AIP Adv. **10**, 075219 (2020).